Engineering Fracture Mechanics 138 (2015) 146–155

Contents lists available at ScienceDirect

Engineering Fracture Mechanics

journal homepage: www.elsevier.com/locate/engfracmech

Investigation of the rate dependence of fracture propagation in rocks using digital image correlation (DIC) method

G. Gao [a], W. Yao [b,c], K. Xia [b,c,*], Z. Li [d]

[a] Institute of Mechanics, Chinese Academy of Sciences, Beijing 100190, China
[b] State Key Laboratory of Hydraulic Engineering Simulation and Safety, School of Civil Engineering, Tianjin University, Tianjin 300072, China
[c] Department of Civil Engineering, University of Toronto, Toronto, Ontario M5S 1A4, Canada
[d] LTCS and College of Engineering, Peking University, Beijing 100871, China

ARTICLE INFO

Article history:
Received 14 January 2015
Accepted 16 February 2015
Available online 2 March 2015

Keywords:
Dynamic fracture toughness
Fracture velocity
Digital image correlation
Loading rate
SHPB
NSCB

ABSTRACT

Loading rate is the main controlling factor in dynamic failure of rocks. In this paper, digital image correlation (DIC) combined with ultra-high speed photography is utilized to study the loading rate effect of a granitic rock – Laurentian granite using notched semi-circular bend (NSCB) method. The dynamic stress intensity factors and crack tip positions are determined from the displacement fields obtained using DIC. Fracture time, fracture toughness and crack growth velocity all exhibit loading rate dependence. The dependence of fracture propagation toughness on crack growth velocity is also obtained, which is in good agreement with that reported in the literature.

1. Introduction

Fracture toughness K_{IC} is a material property that describes the ability of a material containing a crack to resist fracture initiation. There are some standard tests to characterize the fracture initiation behaviors of different materials such as metals [1] and rocks [2–4] under quasi-static loading. The dynamic fracture toughness (DFT) K_{Id} is the critical value of stress intensity factor at the crack initiation point of a specimen subjected to dynamic loading. Investigations have attempted to extend some of the existing static or quasi-static methods for testing fracture toughness to the dynamic fracture tests.

Böhme and Kalthoff [5] first tried to measure the DFT using a three point bending configuration with the load exerted by a drop weight. Tang and Xu [6] measured DFT of rocks through three point bending method using a single Hopkinson bar, and Zhang et al. [7,8] utilized the split Hopkinson pressure bar (SHPB) technique to measure the dynamic rock fracture toughness by using the short rod specimen. However, careful consideration of the inertial effect in dynamic tests was ignored in the calculation of the stress intensity factor and thus the fracture toughness in these studies.

Recently, using the pulse shaping technique [9], Xia and his co-workers [10–12] developed and calibrated a series of fracture testing methods using the modified SHPB technique to characterize the dynamic mode-I fracture toughness of rocks. Among these methods, the notched semi-circular bend (NSCB) method has been proposed by the International Society for Rock Mechanics (ISRM) as a suggested method for determining dynamic mode-I fracture toughness of rocks [13].

* Corresponding author at: State Key Laboratory of Hydraulic Engineering Simulation and Safety, School of Civil Engineering, Tianjin University, Tianjin 300072, China; Department of Civil Engineering, University of Toronto, Toronto, Ontario M5S 1A4, Canada. Tel.: +1 4169785942; fax: +1 416978681.
E-mail address: kaiwen.xia@utoronto.ca (K. Xia).

http://dx.doi.org/10.1016/j.engfracmech.2015.02.021
0013-7944/

Nomenclature

a	crack length
C_S	shear wave speed
G	strain energy release rate
G_{ID}	fracture energy
K	stress intensity factor
$\dot{K}_I$	fracture loading rate
K_I^P	fracture propagation toughness (FPT)
K_{IA}	the fracture arrest toughness which corresponds to K_I^P at zero fracture velocity
K_{IC}	fracture toughness
K_{Id}	dynamic fracture toughness (DFT)
m	constant
u	displacement components of the subset center point O in x direction
v	displacement components of the subset center point O in y direction
v_c	a specific crack propagation velocity
v_l	the limiting fracture velocity
Δx	the distance from point P to point O in x direction
Δy	the distance from point P to point O in y direction
$\frac{\partial u}{\partial x}$	the gradients of displacement components for the subset
$\frac{\partial u}{\partial y}$	the gradients of displacement components for the subset
$\frac{\partial v}{\partial x}$	the gradients of displacement components for the subset
$\frac{\partial v}{\partial y}$	the gradients of displacement components for the subset
DFT	dynamic fracture toughness
DIC	digital image correlation
FPT	fracture propagation toughness
ISRM	International Society of Rock Mechanics
LG	Laurentian granite
NSCB	notched semi-circular bend
PFT	propagation fracture toughness
PMMA	polymethylmethacrylate
SHPB	split Hopkinson pressure bar
SIF	stress intensity factor
ZNCC	zero-normalized cross-correlation
ZOI	zone of interest

In addition to fracture initiation toughness, for dynamic fracture, there is also a fracture propagation toughness (FPT) K_I^P, which is equal to the stress intensity factor K for a propagating fracture. Equivalently, one can define fracture energy G_{ID}, which is equal to the strain energy release rate G for a propagating fracture. FPT describes the material resistance against crack growth.

Owen et al. [14] experimentally monitored the crack propagation and determined the FPT of Aluminum sheet using a series of strain gauges. Bertram and Kalthoff [15] intended to study the FPT of brittle materials including Polymethylmethacrylate (PMMA) and Solnhofen limestone using strain gauges. Xia and his co-workers [10–12] measured the average FPT of rocks using a laser gap gauge system combined with SHPB technique and determined the relation between average FPT and crack growth velocity of Laurentian granite.

The relationship between FPT and the crack propagation velocity has been investigated for photoelastic polymers in several papers [16,17]. Shukla et al. [18] performed a series of dynamic experiments using photoelasticity method to systematically study the relationship between FPT and the crack velocity for different types of polymer specimens. Bertram and Kalthoff [15] obtained the FPT of Solnhofen limestone at different crack propagation velocity using strain gauges. However due to the limitation of available measurement techniques (e.g. strain gauge near the crack tip [19]) for opaque materials and/or the complicated configurations of rock, dynamic fracture parameters especially crack propagation velocity and FPT could not be well determined.

To overcome the above-mentioned obstacles for studying fracture propagation for opaque materials like rocks, we adopted an optical full-field measurement of digital image correlation (DIC). This method has been proven to be a versatile method in our previous work [20]. By applying different levels of impact loading, crack initiated and then propagated at different velocities. The relationship between DFT and the crack growth velocity was obtained.

2. Dynamic fracture tests and extraction of fracture parameters using DIC

2.1. Sample preparation

Laurentian granite (LG), taken from the Laurentian region of Grenville province of the Precambrian Canadian Shield, north of St. Lawrence and north-west of Quebec City, Canada, is chosen as the material in this work [20]. Its physical and mechanical properties have been well characterized in earlier studies [10–12]. The mineral grain size of Laurentian granite varies from 0.2 to 2 mm, where the average quartz grain size of 0.5 mm, the average feldspar grain size of 0.4 mm and Biotite grain size of the order of 0.3 mm. The mineral composition of this rock is dominated by feldspar (60%), followed by quartz (33%) and Biotite (3–5%). The physical and mechanical properties of LG are summarized in Table 1.

Rock cores with a nominal diameter of 56.62 mm were drilled from Laurentian granite block. They were then machined and cut into semi-circular shape with an average thickness of 16 mm. The NSCB specimen in SHPB testing system and the geometry are schematically shown in Fig. 1. P_1 and P_2 are the forces on the incident bar-sample interface and the transmitted bar-sample interface, respectively. A notch, with about 5 mm in length and 0.9 mm in width, was fabricated using a diamond impregnated saw. The distance between the supporting pins S is 38 mm.

According to the suggested optimal speckle pattern and size [21–23], optimal speckle patterns, in our tests, were fabricated by spray painting combined with dot printing to ensure random speckle patterns with desired size and mean intensity gradient. Typical NSCB specimen with speckle patterns is shown in Fig. 2(a), which is sprayed with white paint and alternatively printed with black, red and blue dots (Images here were transferred into grayscale image).

2.2. Experimental setups

The dynamic loading was exerted with a 25 mm diameter SHPB system (as shown in Fig. 3), which contains a gas pressure gun, a striker bar, an incident bar and a transmitted bar. An adapter with two pins (as shown in Fig. 1) was introduced to achieve three-point bending load to the sample. Two pairs of strain gauges were cemented on the incident and transmitted bars to monitor the stress wave history. Their distances away from the bar-sample interfaces are 735 mm and 600 mm for the incident and transmitted bars, respectively. The strain gauge signals were recorded by an eight-channel digital oscilloscope (Model: Sigma 90 by Nicolet). The sampling rate was 10 MHz with the resolution of 12 bits. Pulse shaping technique was adopted to achieve dynamic force balance.

Ultra-high speed framing camera (model: *Ultra UHSi 12/24 IVV Imprint*™) with a spatial resolution of 1082 × 974 pixels at frame rate up to 200 million frames/s was utilized in our tests. This camera can take up to 24 photographs of the specimen deformation process with a resolution of 12 bits. The frame rate used in our tests was 180,000 frames/s with a fixed exposure time of 1 μs in order to clearly observe the propagation of crack in the dynamic fracture tests since crack initiated in less than hundred microseconds [20].

The incident wave signal was used to synchronize the camera and the flash light with the fracture test through a timing delay circuit. A 50 mm f/1.4D camera lens by *Nikon* was used to capture the images. The focus of ultra-high speed camera was manually adjusted under focused mode to obtain images with optimal quality. To protect the camera and the flash light, a high transmission PMMA plate was placed between the specimen and the camera.

The captured images were first processed to enhance image quality and then used for post analysis using MATLAB program to obtain the displacement and strain fields. The accuracy of our program was estimated as 0.01 pixel. Wavelet denoising technology and 2D MATLAB cubic spline interpolation were applied to improve the calculated results of displacement fields [20].

2.3. Fracture parameter extraction

The principle of DIC is to track the same pixel points located in various deformed images using selected correlation function such as zero-normalized cross-correlation (ZNCC) [24]. By maximizing the correlation coefficient, the location of a subimage (a square subset $(2N+1)\times(2N+1)$ centered at the considered point) in the deformed image is detected and the displacement components of this subset center can be determined (Fig. 4). The point $P'(x', y')$ after deformation is related to the coordinate $O(x_0, y_0)$ in reference image as:

$$\begin{aligned} x' &= x_0 + \Delta x + u + \frac{\partial u}{\partial x}\Delta x + \frac{\partial u}{\partial y}\Delta y \\ y' &= y_0 + \Delta y + v + \frac{\partial v}{\partial x}\Delta x + \frac{\partial v}{\partial y}\Delta y \end{aligned} \tag{1}$$

Table 1
The physical and mechanical properties of LG.

Density (g/cm)	Porosity (%)	Young's modulus (GPa)	Poisson's ratio	Tensile strength (MPa)	Compressive strength (MPa)
2.63	0.64	92	0.21	12.8	259

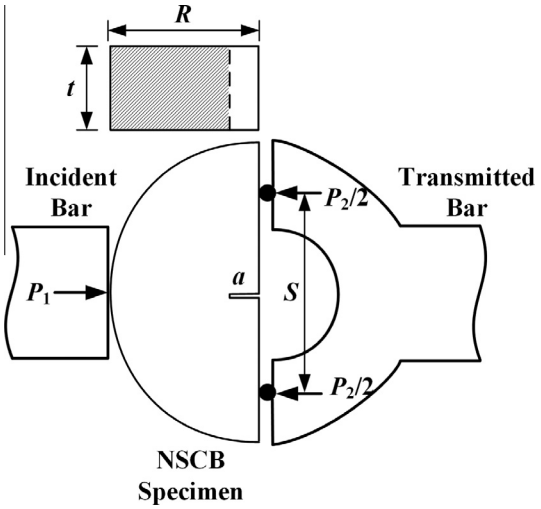

Fig. 1. Schematics of NSCB specimen in SHPB system.

where u, v are the displacement components of the subset center point O in x, y direction, respectively. Δx and Δy are the distance from point P to point O, while $\frac{\partial u}{\partial x}$, $\frac{\partial u}{\partial y}$, $\frac{\partial v}{\partial x}$ and $\frac{\partial v}{\partial y}$ are the gradients of displacement components for the subset.

The horizontal displacement u and vertical displacement v can be determined by optimizing the correlation function. The same tracking procedure is repeated on other points of interest, and the full-field displacement of the zone of interest (ZOI) can thus be obtained. The crack tip location and other fracture parameters, such as the stress intensity factor and the fracture toughness, can be further determined by using the measured displacement fields and the theoretical displacement fields [20].

Fig. 5 shows the ZOI in a typical NSCB test, which is defined for the area around the crack tip and the possible crack path. ZOI has an average dimension of about 23.5 mm × 23.5 mm, with a scale factor of about 90 μm/pixel. The window size for step search was set as 31 × 31 pixels, and the subset size for subpixel estimation was 41 × 41 pixels.

For the mode I, mode II and mixed-mode in plane problems, the displacement fields can be expressed as [25,26]:

$$u = \sum_{n=1}^{\infty} \frac{C_n}{2\mu} r^{n/2} \left[k \cos\frac{n\theta}{2} - \frac{n}{2} \cos\left(\frac{n}{2} - 2\right)\theta + \left(\frac{n}{2} + (-1)^n\right) \cos\frac{n\theta}{2} \right] - \sum_{n=1}^{\infty} \frac{D_n}{2\mu} r^{n/2} \left[k \sin\frac{n\theta}{2} - \frac{n}{2} \sin\left(\frac{n}{2} - 2\right)\theta + \left(\frac{n}{2} - (-1)^n\right) \sin\frac{n\theta}{2} \right] \tag{2}$$

$$v = \sum_{n=1}^{\infty} \frac{C_n}{2\mu} r^{n/2} \left[k \sin\frac{n\theta}{2} + \frac{n}{2} \sin\left(\frac{n}{2} - 2\right)\theta - \left(\frac{n}{2} - (-1)^n\right) \sin\frac{n\theta}{2} \right] - \sum_{n=1}^{\infty} \frac{D_n}{2\mu} r^{n/2} \left[-k \cos\frac{n\theta}{2} - \frac{n}{2} \cos\left(\frac{n}{2} - 2\right)\theta + \left(\frac{n}{2} - (-1)^n\right) \cos\frac{n\theta}{2} \right] \tag{3}$$

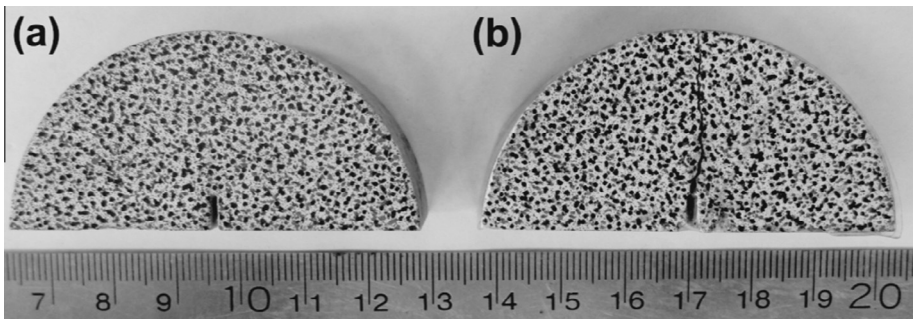

Fig. 2. NSCB specimens with speckle patterns: (a) intact specimen and (b) fractured specimen.

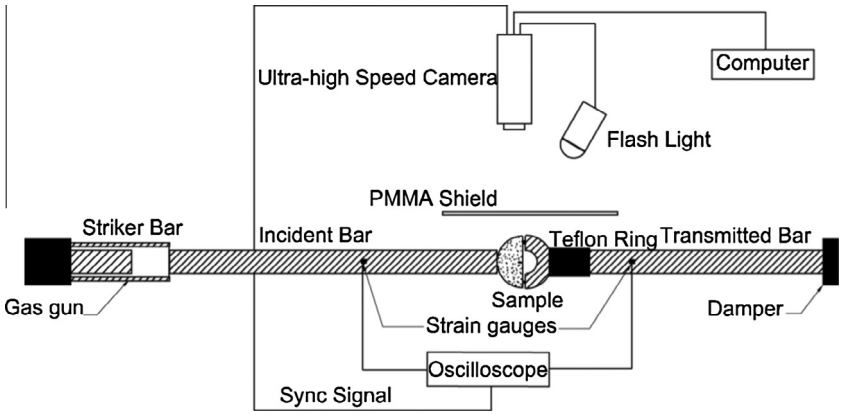

Fig. 3. Schematics of experimental setup.

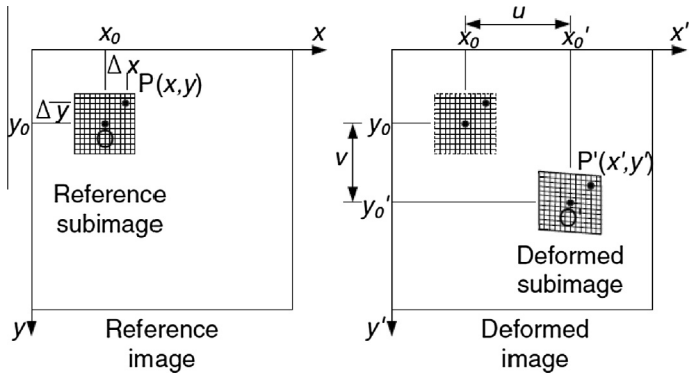

Fig. 4. Schematics of the reference and deformed subimages.

where u and v are displacement components, μ is shear modulus of the material, κ is $(3-v)/(1+v)$ for plane stress and $3-4v$ for plane strain, v is Poisson's ratio of the material, r and θ are polar coordinates around a crack tip. C_n and D_n are parameters to be determined. Particularly, C_1 and D_1 are related to the mode I and mode II stress intensity factors, K_I and K_{II} through relations: $C_1 = \frac{K_I}{\sqrt{2\pi}}$ and $D_1 = -\frac{K_{II}}{\sqrt{2\pi}}$.

Taking account of possible rigid body translation and rotation, the displacement filed can be revised as:

$$u_k = \sum_{n=1}^{N} C_n f_{In}(r_k,\theta_k) - \sum_{n=1}^{\infty} D_n f_{IIn}(r_k,\theta_k) + T_x - Ry_k \tag{4}$$

$$v_k = \sum_{n=1}^{N} C_n g_{In}(r_k,\theta_k) - \sum_{n=1}^{\infty} D_n g_{IIn}(r_k,\theta_k) + T_y + Rx_k \tag{5}$$

where

$$f_{In}(r_k,\theta_k) = \frac{1}{2\mu} r_k^{n/2}\left[\left(\kappa\cos\frac{n\theta_k}{2} - \frac{n}{2}\cos\left(\frac{n}{2}-2\right)\theta_k + \left(\frac{n}{2}+(-1)^n\right)\cos\frac{n\theta_k}{2}\right)\right] \tag{6}$$

$$f_{IIn}(r_k,\theta_k) = \frac{1}{2\mu} r_k^{n/2}\left[\left(\kappa\sin\frac{n\theta_k}{2} - \frac{n}{2}\sin\left(\frac{n}{2}-2\right)\theta_k + \left(\frac{n}{2}-(-1)^n\right)\sin\frac{n\theta_k}{2}\right)\right] \tag{7}$$

$$g_{In}(r_k,\theta_k) = \frac{1}{2\mu} r_k^{n/2}\left[\left(\kappa\sin\frac{n\theta_k}{2} + \frac{n}{2}\sin\left(\frac{n}{2}-2\right)\theta_k - \left(\frac{n}{2}-(-1)^n\right)\sin\frac{n\theta_k}{2}\right)\right] \tag{8}$$

$$g_{IIn}(r_k,\theta_k) = \frac{1}{2\mu} r_k^{n/2}\left[\left(-\kappa\cos\frac{n\theta_k}{2} - \frac{n}{2}\cos\left(\frac{n}{2}-2\right)\theta_k + \left(\frac{n}{2}-(-1)^n\right)\cos\frac{n\theta_k}{2}\right)\right] \tag{9}$$

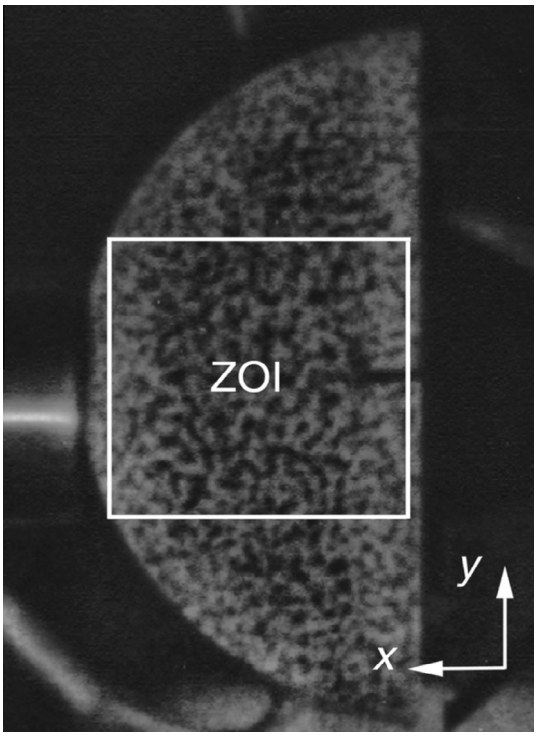

Fig. 5. Typical NSCB specimen with the speckle pattern and its ZOI.

T_x and T_y are the rigid body translation along x and y direction, and R is the rigid body rotation. The subscript k ($k = 1, 2, 3, \ldots, M$) denotes the point number. Eqs. (4) and (5) can be written in matrix form as

$$h = b\Delta \tag{10}$$

where

$$h = \begin{bmatrix} u_1 \\ \cdot \\ \cdot \\ \cdot \\ u_M \\ v_1 \\ \cdot \\ \cdot \\ \cdot \\ v_M \end{bmatrix}, \quad b = \begin{bmatrix} f_{I1} \cdots -f_{II1} \\ \cdot \\ \cdot \\ \cdot \\ f_{IM} \cdots -f_{IIM} \\ g_{I1} \cdots -g_{II1} \\ \cdot \\ \cdot \\ \cdot \\ g_{IM} \cdots -g_{IIM} \end{bmatrix}, \quad \Delta = \begin{bmatrix} C_1 \\ \cdot \\ \cdot \\ \cdot \\ Cm \\ D_1 \\ \cdot \\ \cdot \\ \cdot \\ Dm \end{bmatrix}.$$

Here we assume that the stress intensity factors as well as higher-order terms and the crack tip location are unknowns in Eq. (10). The fracture propagation parameters, including stress intensity factor, crack tip location, higher-order terms in the series expansion of displacement fields, and rigid-body displacement components are determined simultaneously using the regression method of nonlinear least squares [20].

When crack is initiated, the asymptotic expressions for sliding and opening displacements should be modified to include the effect of crack growth velocity. Deng [27] has derived the explicit expressions by considering the steady-state terms and the corresponding transient corrections. However, for slow crack propagation (e.g. $v/C_S < 0.3$, where v is crack propagation velocity and C_S is shear wave velocity), the error for ignoring the crack growth velocity effect is lower than 5% [20]. Four terms were thus included in our following data analysis without compromising the precision and facilitating the regression process.

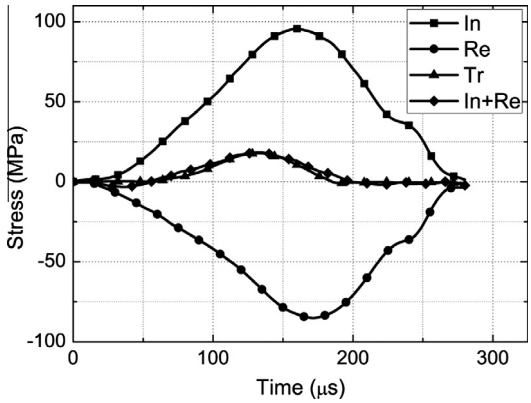

Fig. 6. Typical dynamic force balance during NSCB tests (In: incident wave, Re: reflective wave, Tr: transmitted wave, In + Re: the sum of incident and reflective waves).

3. Results and discussion

3.1. Dynamic force balance

The incident, reflected and transmitted wave were measured using strain gauges and are denoted as ε_i, ε_r and ε_t, respectively. Assuming one-dimensional stress wave propagation in the incident and transmitted bars, the force on both ends of the sample are determined as

$$P_1 = AE(\varepsilon_i + \varepsilon_r), \quad P_2 = AE\varepsilon_t \tag{11}$$

As required in the suggested method of NSCB test, dynamic force balance is needed to guarantee quasi-static stress analysis of specimen [13]. A C11000 copper disc was used to shape the incident wave and achieve dynamic force balance. Dynamic forces on both ends of the specimen and the dynamic force balance from a typical test are shown in Fig. 6. The dynamic force on the incident bar-sample surface P_1 is proportional to the sum of incident (In) and reflected (Re) stress wave, and on the transmitted side P_2 is related to the transmitted (Tr) wave as expressed in Eq. (11). As shown in Fig. 6, the peak values and dynamic force histories on both sides of the sample are almost identical. The dynamic force balance is thus approximately achieved, which makes it possible for quasi-static stress analysis prior to the fracture initiation [13].

3.2. Typical results

Typical intact and fractured NSCB specimens are shown in Fig. 2. With the dynamic force balance and DIC analysis, typical results such crack length and stress intensity factor obtained from dynamic tests are shown in Fig. 7. It can be seen that the crack started to grow at about 140 μs after the incident wave arriving at the specimen, which is manifested by a sudden increase of the crack length. At this time instance, the critical stress intensity factor or the fracture initiation toughness is read as 4.73 MPa $m^{1/2}$. The dynamic stress intensity factor decreases first after crack initiation and then increases continuously to 13.5 MPa $m^{1/2}$.

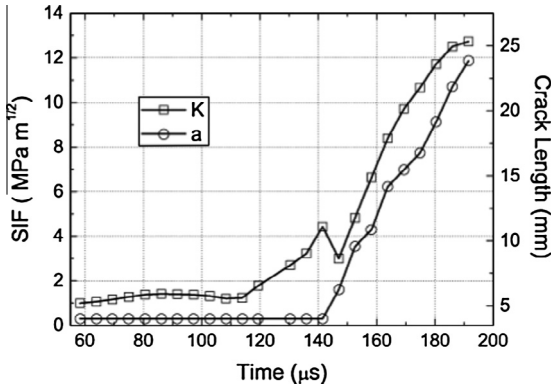

Fig. 7. Evolution of crack length and stress intensity factor in a typical test.

3.3. Rate dependent of fracture parameters

Using the methods described above, several fracture propagation parameters were studied. The first parameter is the fracture time, which is defined as the time span between the arrival of the stress wave and the crack initiation. As shown in Fig. 8, the fracture time declines dramatically with the fracture loading rate ($\dot{K}_I$) for low fracture loading rate, while it remains constant when fracture loading rate reaches up to 200 GPa $m^{1/2}$ s^{-1}. This result can be explained using the microscopic mechanism of dynamic failure. Only a fraction of the total microcracks are involved in rock deformation under lower loading rate. As the loading rate increases, more and more microcracks are involved, until at one point all microcracks are involved in the dynamic failure. After this point, the time to fracture remains the same. This critical point corresponds to the fracture loading rate of 200 GPa $m^{1/2}$ s^{-1}.

The crack propagation velocity could be obtained using crack tip position versus time relation. The results show that average crack propagation velocity varied with loading rates (as shown in Fig. 9). At lower loading rate, average crack growth velocity increases dramatically with the loading rate. However, when the loading rate exceeds 200 GPa $m^{1/2}$ s^{-1}, average crack growth velocity saturates and oscillates around 850 m/s.

It is widely known that a brittle crack cannot propagate faster than the Rayleigh wave speed according to dynamic fracture mechanics [28]. While a shear loading may lead to higher crack speed that even faster than Rayleigh wave speed [29,30], the mode I crack's limiting speed is the Rayleigh speed of the material. In real material tests, the crack speed would be much lower than the limiting crack speed due to loading condition and other factors [31], and the highest average speed we obtained in our tests is about $0.3C_S$ (C_S: shear wave speed).

The fracture initiation toughness also increases with fracture loading rate, especially in the low loading rate range (as shown in Fig. 10). This observation agrees well with that in Ref. [12], and comparison was made and discussed in previous work [20]. The increase rate of fracture toughness becomes slower when the loading rate reaches the critical rate at 200 GPa $m^{1/2}$ s^{-1}.

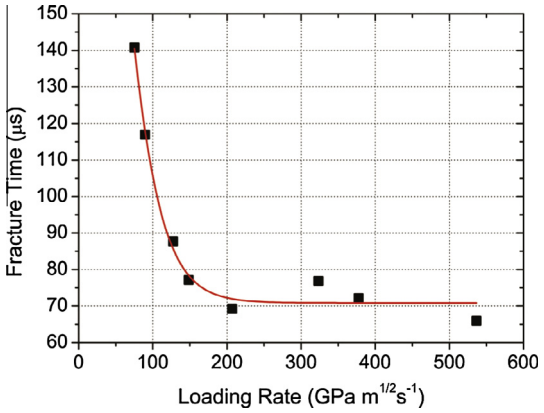

Fig. 8. Fracture time vs. fracture loading rate.

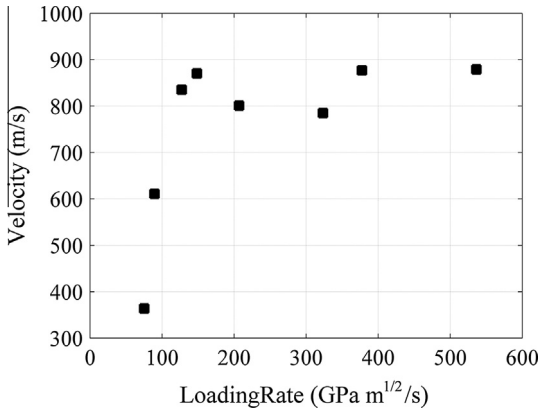

Fig. 9. Average crack growth velocity versus fracture loading rate.

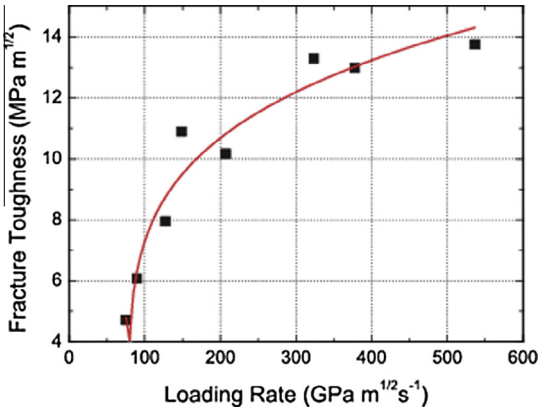

Fig. 10. Fracture initiation toughness vs. fracture loading rate.

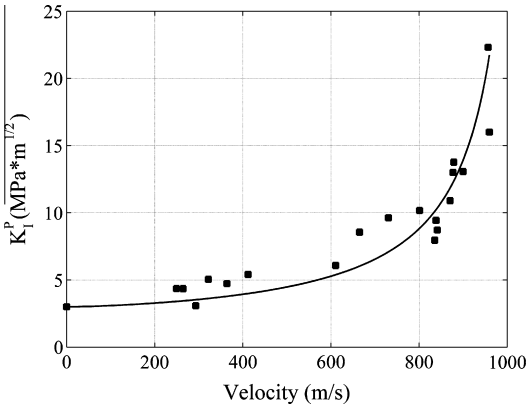

Fig. 11. Variation of fracture propagation toughness with crack growth velocity.

3.4. Fracture propagation toughness vs. velocity

The fracture propagation toughness is believed to be a function of fracture velocity [32]. Shukla et al. [18] discussed the relationship between the stress intensity factor and crack velocity of different types of polymer specimens. Nevertheless, the velocity dependent of fracture propagation toughness in rocks is still lack of evidence.

Fracture propagation toughness, measured in form of the quantity K_I^P, is the stress intensity factor K at a specific crack propagation velocity v_c in a dynamic test. From DIC analysis, the instantaneous crack propagation velocities in dynamic tests are determined. The corresponding time-varying stress intensity factors could also be calculated from the analysis. As shown in Fig. 11, fracture propagation toughness increased with the crack growth velocity. This phenomenon has been observed by Zehnder and Rosakis's [32] for AISI 4340 high strength steel.

Anderson [33] proposed an empirical relationship between fracture velocity and fracture propagation toughness as:

$$K_I^P = \frac{K_{IA}}{1-(v_c/v_l)^m} \tag{12}$$

where m is a constant, v_l is the limiting fracture velocity, and K_{IA} is the fracture arrest toughness which corresponds to K_I^P at zero fracture velocity. Fitting our data into Eq. (12) yields: $K_{IA} = 3$ MPa m$^{1/2}$, $m = 1.47$, $v_l = 1061$ m/s.

The value of K_{IA} as predicted from our results is lower than the averaged fracture initiation toughness obtained above. The limiting velocity predicted here is larger (about $0.38C_S$) than the highest average velocity we measured. This may result from the limitation of the size of the specimen and the range of measurements.

4. Conclusions

An optical full-field measurement of digital image correlation (DIC) was adopted to investigate the dynamic fracture behavior of rocks using notched semi-circular bend specimen loaded by a split Hopkinson pressure bar apparatus.

Laurentian granite was studied using this method to understand the effect of loading rate on the fracture propagation of dynamic fractures in rocks.

The fracture processes under different loading rate recorded by ultra-high speed camera were analyzed using the DIC technique. Dynamic fracture parameters, including the fracture time, fracture velocity and fracture initiation toughness all exhibit obvious loading rate dependence. These fracture parameters all increase with the loading rate. However under higher loading rate, the variation of these variables is less than that under lower loading rate. There exists a critical loading rate beyond which the fracture parameters remain roughly constant.

The relationship between the dynamic fracture propagation toughness and fracture velocity was also obtained for the rock studied. The dynamic fracture propagation toughness increases with the crack propagation velocity and there exists a limiting crack propagation velocity. This limiting velocity is much lower than the theoretical limiting velocity, which is consistent with existing experimental results in the literature for other brittle solids.

Acknowledgements

This work was supported by the Innovative Research Groups of the Natural Science Foundation of China (NSFC) under Grant # 51321065 and the NSFC Grant # 51479131, and the National Basic Research Program of China under Grant # 2010CB731503. K. Xia's research was partially supported by the Natural Sciences and Engineering Research Council of Canada (NSERC) through the Discovery Grant # 72031326.

References

[1] ASTM. Standard test method for linear-elastic plane-strain fracture toughness KIc of metallic materials. ASTM annual book. West Conshohocken: ASTM International; 2012.
[2] Fowell RJ, Hudson JA, Xu C, Chen JF. Suggested method for determining mode-I fracture-toughness using cracked chevron-notched Brazilian Disc (CCNBD) Specimens. Int J Rock Mech Min 1995;32(1):57–64.
[3] Kuruppu MD, Obara Y, Ayatollahi MR, Chong KP, Funatsu T. ISRM-Suggested method for determining the mode I static fracture toughness using semi-circular bend specimen. Rock Mech Rock Eng 2014;47(1):267–74.
[4] Ouchterlony F. Suggested methods for determining the fracture toughness of rock. Int J Rock Mech Min 1988;25(2):71–96.
[5] Böhme W, Kalthoff JF. The behavior of notched bend specimens in impact testing. Int J Fract 1982;20(4):R139–43.
[6] Tang CN, Xu XH. A new method for measuring dynamic fracture-toughness of rock. Eng Fract Mech 1990;35(4–5):783–91.
[7] Zhang ZX, Kou SQ, Jiang LG, Lindqvist PA. Effects of loading rate on rock fracture: fracture characteristics and energy partitioning. Int J Rock Mech Min Sci 2000;37(5):745–62.
[8] Zhang ZX, Kou SQ, Yu J, Yu Y, Jiang LG, Lindqvist PA. Effects of loading rate on rock fracture. Int J Rock Mech Min Sci 1999;36(5):597–611.
[9] Frew DJ, Forrestal MJ, Chen W. Pulse shaping techniques for testing brittle materials with a split Hopkinson pressure bar. Exp Mech 2002;42(1):93–106.
[10] Chen R, Xia K, Dai F, Lu F, Luo SN. Determination of dynamic fracture parameters using a semi-circular bend technique in split Hopkinson pressure bar testing. Eng Fract Mech 2009;76(9):1268–76.
[11] Dai F, Chen R, Iqbal MJ, Xia K. Dynamic cracked chevron notched Brazilian disc method for measuring rock fracture parameters. Int J Rock Mech Min 2010;47(4):606–13.
[12] Dai F, Xia K, Zheng H, Wang YX. Determination of dynamic rock mode-I fracture parameters using cracked chevron notched semi-circular bend specimen. Eng Fract Mech 2011;78(15):2633–44.
[13] Zhou YX, Xia K, Li XB, Li HB, Ma GW, Zhao J, et al. Suggested methods for determining the dynamic strength parameters and mode-I fracture toughness of rock materials. Int J Rock Mech Min 2012;49:105–12.
[14] Owen DM, Zhuang S, Rosakis AJ, Ravichandran G. Experimental determination of dynamic crack initiation and propagation fracture toughness in thin aluminum sheets. Int J Fract 1998;90(1–2):153–74.
[15] Bertram A, Kalthoff JF. Crack propagation toughness of rock for the range of low to very high crack speeds. Key Eng Mat 2003;251-2:423–30.
[16] Ravi-Chandar K, Knauss WG. An experimental investigation into dynamic fracture: I. Crack initiation and arrest. Int J Fract 1984;25(4):247–62.
[17] Ravi-Chandar K, Knauss WG. An experimental investigation into dynamic fracture: III. On steady-state crack propagation and crack branching. Int J Fract 1984;26(2):141–54.
[18] Shukla A, Nigam H. A note on the stress intensity factor and crack velocity relationship for Homalite-100. Eng Fract Mech 1986;25(1):91–102.
[19] Dally JW, Sanford RJ. Strain-gage methods for measuring the opening-mode stress-intensity factor. KI Exp Mech 1987;27(4):381–8.
[20] Gao G, Huang S, Xia K, Li Z. Application of digital image correlation (DIC) in dynamic notched semi-circular bend (NSCB) tests. Exp Mech 2014:1–10.
[21] Pan B, Lu Z, Xie H. Mean intensity gradient: an effective global parameter for quality assessment of the speckle patterns used in digital image correlation. Opt Lasers Eng 2010;48(4):469–77.
[22] Sutton MA, Li N, Garcia D, Cornille N, Orteu JJ, McNeill SR, et al. Scanning electron microscopy for quantitative small and large deformation measurements part II: experimental validation for magnifications from 200 to 10,000. Exp Mech 2007;47(6):789–804.
[23] Sutton MA, Orteu J-J, Schreier H. Image correlation for shape, motion and deformation measurements: basic concepts, theory and applications. New York: Springer; 2009.
[24] Pan B, Qian KM, Xie HM, Asundi A. Two-dimensional digital image correlation for in-plane displacement and strain measurement: a review. Meas Sci Technol 2009;20(6):1–17.
[25] Zhang R, He L. Measurement of mixed-mode stress intensity factors using digital image correlation method. Opt Lasers Eng 2012;50(7):1001–7.
[26] Yoneyama S, Morimoto Y, Takashi M. Automatic evaluation of mixed-mode stress intensity factors utilizing digital image correlation. Strain 2006;42(1):21–9.
[27] Deng X. Transient, asymptotic, elastodynamic analysis a simple method and its application to mixed-mode crack growth. Int J Solid Struct 1993;30(4):513–9.
[28] Freund LB. Dynamic fracture mechanics. Cambridge: Cambridge University Press; 1990.
[29] Abraham FF, Gao H. How fast can cracks propagate? Phys Rev Lett 2000;84(14):3113–6.
[30] Rosakis AJ, Samudrala O, Coker D. Cracks faster than the shear wave speed. Science 1999;284(5418):1337–40.
[31] Gao HJ. A theory of local limiting speed in dynamic fracture. J Mech Phys Solids 1996;44(9):1453–74.
[32] Zehnder A, Rosakis A. Dynamic fracture initiation and propagation in 4340 steel under impact loading. Int J Fract 1990;43(4):271–85.
[33] Anderson TL. Fracture mechanics: fundamentals and applications. CRC Press; 2005.